A Thermally Powered ISFET Array for On-body pH Measurement

Matthew Douthwaite, *Student Member, IEEE*, Ermis Koutsos, *Student Member, IEEE*, David C. Yates, *Member, IEEE*, Paul D. Mitcheson, *Senior Member, IEEE* and Pantelis Georgiou, *Senior Member, IEEE*

Abstract—Recent advances in electronics and electrochemical sensors have led to an emerging class of next generation wearables, detecting analytes in bio-fluids such as perspiration. Most of these devices utilise ion-selective electrodes (ISEs) as a detection method, however ion sensitive field effect transistors (ISFETs) offer a solution with improved integration and a low power consumption. This work presents a wearable, thermoelectrically powered system composed of an application specific integrated circuit (ASIC), two commercial power management integrated circuits (ICs) and a network of commercial thermoelectric generators (TEGs). The ASIC is fabricated in 0.35 μm CMOS and contains an ISFET array designed to read pH as a current, a processing module which averages the signal to reduce noise and encodes it into a frequency, and a transmitter. The output frequency has a measured sensitivity of 6 to 8 kHz/pH for a pH range of 7 to 5. It is shown that the sensing array and processing module has a power consumption 6 μW, and therefore can be entirely powered by body heat using a TEG. Array averaging is shown to reduce noise at these low power levels to 104 μV (input referred integrated noise), reducing the minimum detectable limit of the ASIC to 0.008 pH units. The work forms the foundation and proves the feasibility of battery-less, on-body electrochemical for perspiration analysis in sports science and healthcare applications.

Index Terms—CMOS integrated Sensors, ISFET, pH measurement, sensor arrays, thermoelectric generators

I. INTRODUCTION

Wearable health and fitness devices have become a prevalent choice for monitoring daily activity and physiological status remotely. This class of technology presents an opportunity to enable continuous and remote observation of patients outside the hospital environment and athletes during training. However, mainstream devices are limited as they only observe physical activity and electrophysiological signals such as heart rate (ECG) or muscle activity (EMG) [1]. As reported by [2], there is scope to greatly improve the obtainable information on a subject through complimenting these observations with electrochemical sensors. The reliance of modern medicine on blood tests is evidence of the importance of analysing and understanding chemical and biological markers in the body. Conveniently, many of the useful markers which exist in blood are also observable in bio-fluids, such as perspiration, saliva,

M. Douthwaite, E. Koutsos and P. Georgiou are with the Centre for Bio-Inspired Technology, Institute of Biomedical Engineering and the Department of Electrical and Electronic Engineering at Imperial College London, SW7 2AZ, UK (email: {mdouthwaite, ekoutsos, pantelis}@imperial.ac.uk).

D. Yates and P. Mitcheson are with the Department of Electrical and Electronic Engineering, Imperial College London, SW7 2AZ, UK(email: {david.yates, paul.mitcheson }imperial.ac.uk).
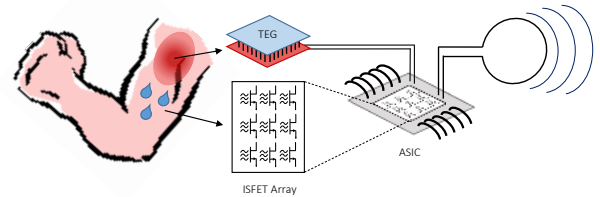
Fig. 1: Illustration of concept. A thermoelectric generator (TEG) and an ISFET array on an ASIC in contact with the skin extract thermal energy and analyse perspiration respectively. The ASIC also contains a processing module and transmitter connected to an off-chip antenna.

tears and urine [3], [4]. This has sparked rapidly growing interest into developing wearable electrochemical sensors, which perform detection and analysis of a range of ions and metabolites. For example, useful measurable properties of perspiration include pH and concentrations of sodium, potassium, glucose and lactate to name a few [5]–[11]. Such devices need to be small, low power and reliable in the first instance, and there are a great many challenges to overcome in both electro-chemistry and electronics before they shall be ready for wide public use [1]. This work describes improvements in the area of power and sensitivity of electrochemical wearables, targeting in particular skin-worn sensors.

The most common detection method is screen-printed ion-selective electrodes (ISEs) [6]–[11]. This technique requires functionalising an electrode for the specific analyte, and then measuring either the voltage (potentiometry) or current flow (amperometry) between this working electrode and a reference electrode. However, while ISEs are a standard method of conducting electrochemical measurements, an alternative is to use ion sensitive field effect transistors (ISFETs). These devices can be manufactured in CMOS in the same manner as a MOSFET, but with their gate contact extended to the top metal layer surface [12], [13]. This becomes the sensing area capacitively coupled to a solution through the Si_3N_4 insulating layer, such that an increase in the charge of the target solution causes current flow through the device. ISFETs in electrochemical wearables have not been widely explored; to the authors' knowledge only two examples exists. Cazale *et. al.* study ISFETs for the application of detecting sodium in perspiration [5] while Nakata *et.al.* monitor the pH of perspiration and skin temperature [14]. Both works show promising results in the use of ISFETs in on-body applications, however they focus on the sensor only. Consequently, these devices are not integrated in CMOS and the works do not

consider the accompanying processing circuitry and power requirements that are necessary for an on-body system.

The monolithic nature of CMOS integrated ISFETs may make them preferable to ISEs. The sensors are fully integrated with the associated instrumentation and processing, allowing optimisation of signals and noise reduction whilst operating with very low electrical currents. Established CMOS manufacturing techniques make this a low-cost and highly scalable solution. Through these attributes one can easily construct arrays, which allow further exploitation to boost signal to noise ratio [13]. As with ISEs, the target solution needs to be biased and a planar integrated reference electrode can be added to a CMOS chip through post-processing.

A key limitation of modern wearables is their dependency on batteries as a power supply, which leads to bulky and more expensive systems. However there are alternative solutions such as wireless powering or energy harvesting. A potential solution is the harvesting of thermal energy emitted by the human body. This has the advantage over other sources such as kinetic or solar as moving parts are not required, usage can be indoors 24 hours a day [15] and thermal harvesters have been shown to provide a greater power per unit volume than their kinetic equivalent in a normal walking scenario [16]. While the energy available from this source is very small, if harnessed it could allow a sensing device to be more independent, monitor indefinitely and potentially reduce cost. Using ISFETs integrated with instrumentation in CMOS, a device like this can operate under such strict power budgets, making energy harvesting feasible.

The main contribution of this work is the first integrated CMOS ISFET sensing array powered by thermoelectric generators (TEGs), as illustrated in Fig. 1. This is enabled due to the mechanisms presented in this work; the capability to operate the sensors in weak inversion to achieve low power operation and the capability to perform array averaging of the current-mode signal which decreases signal noise caused by the restrictive power budget. As a result, the limit of detection of the module is improved compared to a single sensor. A summary of design considerations for an on-body thermally powered device and suitable commercially available TEGs and power management integrated circuits (ICs) for this application is also provided. We demonstrate a system which allows a custom application specific integrated circuit (ASIC) to be powered by TEGs which harvest body heat, providing a functional proof of concept for a body-worn ISFET sensing array for pH measurements. The complete system and its sub-modules are shown in Fig. 2.

The paper is organised as follows. Section II describes the design considerations for harvesting thermal energy at low temperature gradients and the chemical considerations for on-body pH measurements. Section III then describes the ASIC architecture as a whole before explaining each sub-module in detail. Finally, Section IV presents the complete thermoelectric system along with measured results and analysis. Section V discusses conclusions and future work.

II. DESIGN CONSIDERATIONS

In order to optimally design an ASIC to be powered by body heat, the realistically achievable power budget should be explored. The following section explains the process and considerations for selecting a TEG and associated components for a body-worn thermoelectric powered system. Additionally the sensor requirements for an electrochemical device located on the skin are discussed.

A. Thermoelectric Generator (TEG) Selection for Body Worn Applications

A thermoelectric generator (TEG) utilises the Seebeck effect to generate an electric current in the presence of a temperature differential. The 'hot-side' and 'cold-side' must establish a sufficient gradient (ΔT) across the semiconductor device to generate current in a set of alternating n-type and p-type thermocouples, which are connected thermally in parallel but electrically in series. Using these generators for body-worn applications is challenging, as they are usually designed for industrial applications ($\Delta T > 70$ °C), whereas the gradient between human skin and the ambient environment is often less than 10°C [17]. The power extracted can however be maximised through thermal and electrical impedance matching [18]. The ideal maximum power output of a TEG is related to the allowable generator volume, which is of course limited in a wearable device. According to [16], the power output for a volume of 1cm^3 would give us a challenging power budget of 6 µW. Assuming an acceptable volume is in the order of 2 cm^3, a TEG could provide at least 10µW, which gives us a working power budget. This places a strict limit on the design and its abilities. Additionally, the usual voltage output of a TEG in low differential temperature applications is in the order of tens of millivolts, which provides a further challenge. Since, at this stage, the scope of this work does not include the design of an on-chip regulator, a pair of off-chip commercial ICs (The LTC3108 and the LT3009, both from Texas Instruments, described in Section II-B) are used to harvest the energy from the TEG at their low output voltage and provide a stable reference for the ASIC. To reduce the power that has to be used for boosting the voltage and to help the achieve the power budget in general, the ASIC has been designed to operate with a supply of 1.2 V. It is important to note here that the selected harvester IC operates with a high ratio (1:100) step up transformer, allowing it to cold start from voltages as low as 20 mV, which is a feasible target for a body-worn TEG. Another feature of the IC is that it adjusts its input impedance to improve matching and obtain the maximum power from the energy source. A further requirement to improve the power output of the TEG is a heat sink, which helps to cool the cold side of the TEG and thus improves the temperature gradient and therefore the voltage generated. Using the models presented in [18] and the literature, calculations can be carried out to identify an appropriate off-the-shelf TEG for the body-worn application. The models and assumptions used for this study are given in the Appendix. Ultimately, it would be desirable to manufacture a bespoke TEG as the physical parameters could be optimised
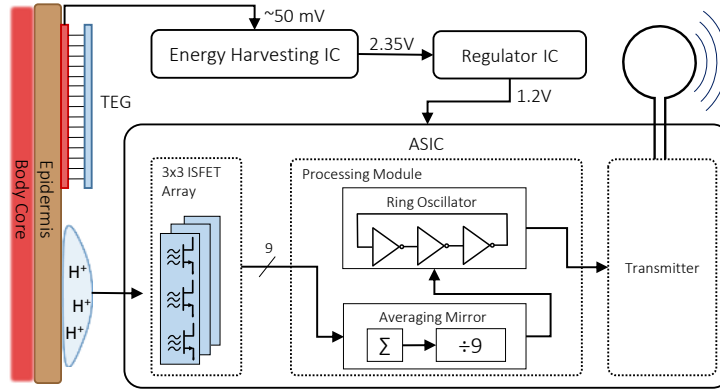
Fig. 2: A diagram of the presented system, showing the application set-up of an on-body TEG and skin-facing sensor, the main components of the ASIC and the power management ICs.

to maximise power extracted in low differential temperature applications and the device could even be made flexible [19], however in this instance commercial TEGs represent a low-cost proof of concept. The most suitable candidate TEGs found which met the minimum loaded voltage of 20 mV are shown in Table I. The devices are evaluated in terms of physical size and maximum power per unit area, using the thermal model described the Appendix. The core body and ambient temperatures (T_B and T_A) used were 37 °C and 24 °C respectively and it was assumed that the electrical matching with the harvester IC would be ideal. As a typical metal heat sink is undesirable for wearable applications, a series of small form factor ceramic heat sinks were identified for use in the thermal sub-system (AMEC THERMASOL, MPC202025T). The thermal impedance of these heat sinks is $R_{th} = 10.21$ K W^{-1} for 15 and 20 mm^2.

The first TEG in Table I shows the Ferrotec module used by Lossec *et.al.* in their study of maximising output power from a body-worn TEG [18]. While the voltage supply and power are unquestionably high, the module size is quite large for a body-worn application and would not achieve a good contact if worn on the wrist as suggested previously. An alternative option from Ferrotec is more a appropriate size just over 4 cm^2, produces a reasonable output voltage and has more than twice the power per unit area. Options from Adaptive and Multicomp were also considered, and the latter was chosen due to its dimensions of 20 x 20 x 3.8 mm, which match the available heat sink size. With the heat sink, the dimensions of the generator is 20 x 20 x 5.3 mm, meaning the height above the surface of the skin is similar to a typical wristwatch and therefore acceptable.

It was discovered in testing that although the minimum cold-start voltage for the harvester IC is given as 20 mV, the TEG from Multicomp could not support the system. As a result, testing was performed with four of these devices in series to produce a larger voltage and to ensure that the harvester IC can operate. It is noted that although a single TEG of equivalent total area could be used for a lower cost, using multiple small modules allows better flexibility of a wearable device and therefore contact with the skin, thus improving the

energy transfer. As this is not accounted for in the calculations it could lead to an overall better performance for a network of small TEGs.

B. Off-Chip Power Management Integrated Circuits

In order to allow the ASIC to be powered reliably via body heat, the low voltage output of a thermoelectric generator needs to be boosted to the required level and the excess power should be stored in case of a drop in supply (for example if the ambient temperature rises or air flow drops). An ultra-low voltage energy harvester, the LTC3108 was selected for this task, which boosts input voltages as low as 20 mV up to a minimum output of 2.35 V. The LTC3108 requires a small external transformer (This design uses the LPR6235-752S from Coilcraft, area 6x6 mm, turns ratio 1:100) and a 1500 µF storage capacitor is also used. The storage capacitor enables the harvestor to store excess energy from the TEGs when there is a surplus. This stored energy can then be used if the temperature gradient across the TEGs drops or for temporary increases in power such as a transmit pulse. A regulator is then required to produce 1.2 V for the chip, and for this the LT3009 was selected. While using these two chips in series is far from optimal (together their efficiency is calculated to be approximately 15%), in future designs custom boost circuitry could be implemented to boost the TEG voltage up to 1.2 V in a single step for reduced losses.

C. Further Considerations for Body-Worn Thermoelectric Generators (TEGs) Placement

Suarez *et.al.* provide a comprehensive investigation into the challenges in body worn TEGs [19]. They show that while the forehead provides the greatest skin temperature, the forearm provides a lower thermal impedance to the body when tightly attached to the skin. This suggests one of the best target area for a thermally powered wearable is the forearm, which is consistent with historical efforts to create thermally powered watches. Additionally, to ensure appropriate convection over the cold side of the TEG, the device would have to be worn on part of the body which is usually exposed to the air and preferably mobile, for example the arms or lower legs [19].

TABLE I: A table of candidate thermoelectric generators with predicted output power when used with the proposed power management ICs.

Manufacturer	Product Code	Dimensions (LxWxH) (mm)	Output Voltage at $R_G = R_L$ (mV)	Calculated Maximum Power (µW)	Power per unit Area (µW cm^{-2})
Ferrotec	450-0.8-3.0	54.4 x 55.5 x 3.4	141.74	1165.84	38.61
Ferrotec	9501/071/040 B	22.4 x 22.4 x 3.18	26.78	292.62	58.32
Adaptive	ET-071-08-15-RS	18 x 18 x 3.8	28.61	204.69	63.18
Multicomp	MPCE-071-10-15	20 x 20 x 3.8	24.11	211.36	52.84
Multicomp	MPCE-071-10-15 (Four in series)	80 x 20 x 3.8	79.08	568.51	52.84

Webb provides average skin temperatures for different areas of the body [17], with the forearm reported as 34 °C in a 27 °C room and 26.9 °C in a 15 °C room. Independently we measured the skin temperature of the forearm in a 23 °C room to be approximately 29 °C, and this has been used for bench testing in the lab.

D. Considerations for On-body pH Measurement

The pH of perspiration correlates to sodium concentration and perspiration rate and is known to vary between a pH of 5 and 7.5 as the rate of production increases, due to the partitioning of charged ions from the body affecting the acidity of the fluid [6], [20], [21]. As a result pH represents an informative and easily observable parameter on which to test our system. The sensitivity of ISFETs to pH is given by the Nernst Equation and is ideally 59 mV/pH. In practice the attainable sensitivity using an ISFET in unmodified CMOS is less than this, closer to 50mV/pH [22], [23], so for a pH range of 5 to 7.5, the design should accommodate a change in V_{chem} of at least 125 mV. To make certain we characterise the full range of operation, we consider a ΔV_{chem} of 180 mV when designing the ISFET front end.

III. DESCRIPTION OF AN ASIC FOR pH TO FREQUENCY CONVERSION

This section describes the design of the CMOS integrated circuits central to the on-body thermally powered system.

A. Top-level Architecture

The top level architecture of the ASIC consists of an ISFET sensing array and a processing module which is made up of a current averaging mirror and ring oscillator for conversion of the analogue array output to a digital signal. A Beta Multiplier is used to create a current bias. The array consists of nine pixels, each with a current output which are added together through a single connection to the current mirror. The output of the mirror divides down the signal giving an average of the array output. The current-mode signal is then converted to a digital pulse using a current starved ring-oscillator. This produces a pulse train with a frequency proportional to the current supplied by the array. A buffer ensures that the oscillator remains unloaded and can drive a custom transmitter oscillating in the ISM band.

B. ISFET Pixel

The sensing array consists of nine ISFETs, each in its own pixel in a 3-by-3 arrangement. This number of pixels has been chosen to balance the benefits of noise reduction due to averaging with the increased power consumption brought a larger array. The pixel architecture is shown in Fig. 3a. The pixel is based on the voltage clamped ISFET architecture, described in [24], which ensures that the voltage at the drain of the ISFET, point X in the figure, is held stable. As a result any change in potential at the floating gate, V_{fg}, will cause a change in current, i_{ds}.

The key element of this design is that, in order to minimise power consumption, the ISFET is kept in weak inversion by supplying a bias current of 1nA. Consequently, if we express the gate voltage of the ISFET, V_{GS}, the sum of the floating gate voltage (with respect to the source) and the potential due to the chemical solution, V_{chem}, then the relationship between V_{GS} and i_{ds} is exponential and, assuming $V_{DS} > 4U_T$, is given by (1) [12], [13], [25]. The relationship between the pH and V_{chem} is shown in (2), where I_0 is the device quiescent drain current, γ represents a chemical offset independent of pH, α is the capacitive division due to the chemical and silicon layers and represents the deviation from the ideal Nernstian sensitivity and U_T is the thermal voltage.

$$I_{ds} = I_0 \exp^{\frac{V_{GS} - V_{chem}}{nU_T}} \quad (1)$$

$$V_{chem} = \gamma + 2.3\alpha U_T pH \quad (2)$$

A further benefit of using ISFETs in weak inversion is that the temperature dependence of pH is eliminated by substituting (2) into (1) [26]. The remaining temperature dependence of the pixel is the same as that in a standard MOSFET in weak inversion. Through simulation we have observed that the temperature dependence of our MOSFETs at the relatively low temperatures expected is close to linear, meaning that is straight forward to compensate for these variations in future, but at the expense of an increased power consumption.

A problem with ISFETs is the accumulation of trapped charge at the floating gate [12]. This can be compensated by using a programmable gate architecture [27], where a ramp voltage input which is capacitively coupled to the gate of the ISFET allows trapped charge cancellation and also enables the bias point of the pixel to be set, giving an adjustable operating region.

The output current of the pixel is mirrored to a node shared between the array, so that a summation is obtained. To ensure the accuracy of the mirrored current, a low-voltage cascode
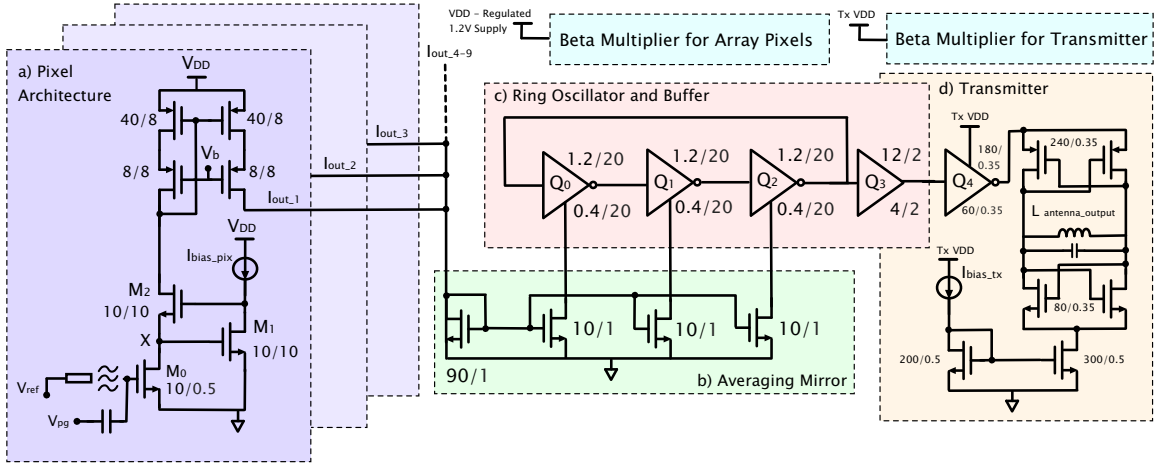
Fig. 3: Schematic of the ASIC. a) shows the architecture of each pixel in the 3-by-3 array. b) and c) make up the processing module, an averaging mirror and ring oscillator with output buffer respectively. The output transmitter is shown in d).

mirror was used, as shown in Fig. 3a. Each pixel has a sensing area of 64µm x 54µm, which is equal to the size of the pixel layout area.

C. Pixel Averaging for Noise Reduction

The output of each pixel is connected to the input of a single current mirror, with a ratio of 9:1 to perform an averaging operation, shown in Fig. 3b. Averaging of the array is important due to the use of very low currents to be in the ISFETs - necessitated by the constrictive power budget of the ASIC - which are by nature more susceptible to uncorrelated noise. Averaging the output of a sensing array will provide a more robust reading of the local target area, minimising uncorrelated noise in comparison to a single sensor for the same overall power consumption. The contributions at low frequency operation are mainly due to thermal and 1/f noise.

Applying the Central Limit Theorem, it can be shown that as a result of creating an array of averaged sensors, reduces the uncorrelated noise by $\sqrt{n}$. Consequently, the uncorrelated noise of the 3-by-3 array is reduced by $\sqrt{9}$.

It should be noted that 1/f noise is not reduced by averaging, which highlights that a future development of the array could be to use a sampling methodology to further improve SNR. Additionally, an electrochemical sensor will also suffer from chemical noise, which we also expect to be reduced by this averaging technique [28].

D. Ring-Oscillator

The ring-oscillator is a simple positive feedback oscillator constructed from an odd number of inverters in a closed loop. They are simple to construct in CMOS, operate with a low voltage and power consumption and the frequency of oscillation can be electrically tuned [29]. Tuning is achieved by regulating the current flowing through the inverters, which affects their switching speed. While the frequency saturates when approaching the maximum current flow, the relationship can be approximated as linear at lower currents [30].
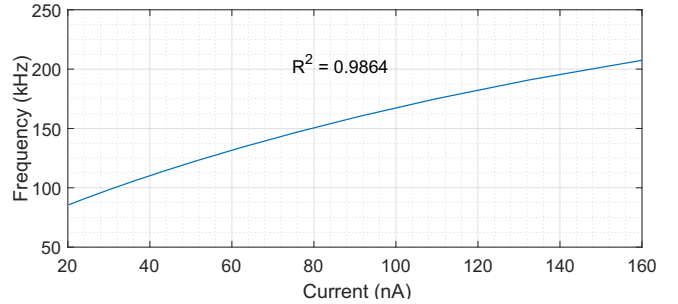

Fig. 4: Relationship between current supplied to ring oscillator and output frequency

In this design a 3 stage ring-oscillator has been used, shown in Fig. 3c, with a maximum frequency of 472kHz with no current starving. The operation is limited to 50 to 250 kHz, where the R^2 value of the relationship is calculated to be 0.9864. This frequency range was chosen as it is three orders of magnitude slower than standard ISM band transmission at 433 MHz and the signal can therefore be used to modulate a signal of that frequency. The relationship between input current and output frequency is shown in Fig. 4.

E. Transmitter

To transmit the information from the device, we chose a simple cross-coupled differential oscillator to generate a carrier signal for the ring oscillator output. It oscillates at 433 MHz using a single loop antenna of diameter 20 mm as the inductor. The supply of the transmitter is connected through another buffer to the output of the ring oscillator, such that the carrier signal is modulated by on-off-keying (OOK). These key signals are shown in the timing diagram in Fig. 5, where a rise in chemical potential, V_{chem}, - representing a rise in pH - is seen at the ISFET gate and causes an increase in the output frequency of the ring oscillator. The transmitter is subsequently modulated by the ring oscillator using OOK. The maximum start-up time for the transmitter is 1 µs.

The power consumption of the transmitter is not optimal at this time and so this section of the ASIC has its own separate
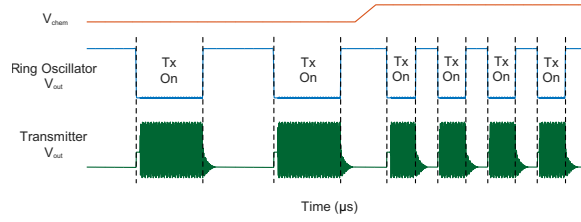
Fig. 5: A simulated timing diagram showing a ramp in chemical potential, V_{chem}, which is seen after a capacitive division at the gate. The ramp causes an increase in ring oscillator frequency, and the output of this stage modulates the transmitter through on-off-keying.
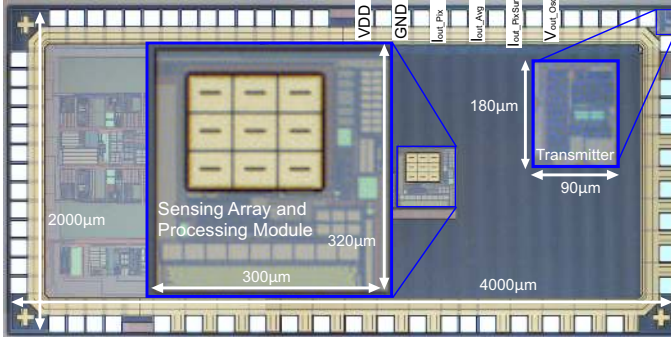

Fig. 6: A micro-photograph of the chip with the sensors, processing module and transmitter highlighted. Key bond pads are also labelled.

supply pad so as not to prevent the main sensing and processing modules from being powered thermally. The output of the ring oscillator is connected externally and therefore a lower power or even passive form of transmission can be implemented as an alternative.

IV. FABRICATED PROTOTYPE AND MEASURED RESULTS

The ASIC has been fabricated in a 0.35μm CMOS process. Fig. 6 shows the chip micro-photograph with the sensing array, processing module and transmitter enlarged. The ASIC operates at 1.2 V supply current, and occupies an area of 0.1089mm^2. The transmitter also operates at 1.2 V and has an area of 0.0128mm^2.

A. Testing Methodology

The ASIC has been fully characterised in both dry and wet conditions. In dry conditions, the ISFET floating gates were biased through the global programmable gate capacitor. In wet testing, the ISFET gates were characterised through a target solution using a silver/ silver chloride (Ag/AgCl) reference electrode. For initial tests, the solution used was distilled water, before pH buffers were used to measure chemical sensitivity.

A printed circuit board (PCB) was designed to interface with the chip for initial testing and characterisation. The PCB holds the harvester and regulator ICs and their associated circuitry, described in Section II-B, as well as test points for interfacing with the ASIC, which is itself bonded to a smaller PCB for easy replacement and repeat testing.

The ASIC was designed with a number of test pads for reading outputs after each sub-module. The key test pads are
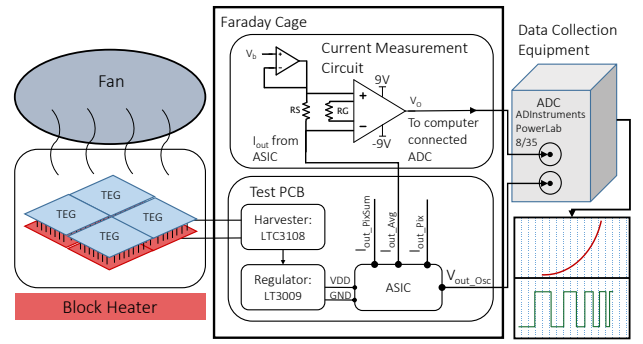

Fig. 7: Diagram of the test set-up used to record and analyse the noise of the ISFET sensors before and after averaging and measure the frequency output of the ring oscillator (the output of the processing module). ASIC connections are labelled to correspond to the pad labels in Fig 6.

the individual pixel current output (each pixel in the array can be selected using a multiplexer), the sum of currents from all the pixels in the sensing array, the average of this output current and the voltage output of the ring oscillator, as shown in Fig. 6. For characterisation of the pixels (Section IV-B) and pH sensitivity of the sensing array (Section IV-D), the ASIC was probed directly using a Keithley 4200-SCS to provide precise inputs and measurements. However, this machine was not suitable for frequency analysis, so an analogue-to-digital converter (ADC) - the ADInstruments PowerLab 8/35 - was used to measure and record the noise (Section IV-C) and output frequency (Section IV-G) of the ASIC. The ADC was connected to a computer to accurately record voltages from the chip at the test points, without the introduction of noise or errors due to transmission. As the output of the pixels and sensing array are current-mode signals, an instrumentation amplifier was used to convert this signal into a voltage to be read by the ADC. The instrumentation amplifier was battery powered as it is purely included for characterisation and is not intended to be part of the final system. Furthermore, using a DC source rather than a mains supply minimises the noise introduced by this conversion stage. The test set-up for Sections IV-C and IV-G is shown in Fig. 7 and the set-up of the measuring instruments is described in more detail in these sections.

B. Pixel Characterisation

The pixels were initially characterised by applying a voltage sweep to the input terminal of the ASIC using the Keithley. The recorded I_d-V_{gs} sweeps showed an exponential response between the pixel output current and both the programmable gate (pg) and reference electrode as expected. Fig. 8 shows the I_d-V_{pg} sweeps of the nine pixels individually and the array average, with V_{pg} applied to the programmable gate terminal, see the schematic in Fig. 3a). The curves are distributed over a 100 mV range, which is due to the trapped charge phenomenon and mismatch. Ideally all ten curves would line up, however the spread here is relatively small, so the averaging forms a good approximation. The pixels saturate at around 450 nA predicted in simulation due to the devices entering strong inversion.
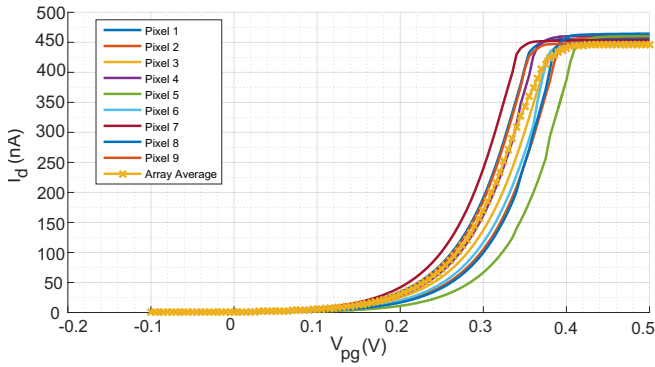
Fig. 8: I_d-V_{pg} Curves for the nine pixels and the array average

The pixels were characterised again using biasing through the reference electrode. A solution of distilled water was applied to the surface and the reference electrode was swept. As expected, the curves showed significantly reduced sensitivity through the solution and Si_3N_4.

C. Noise Analysis of the Sensing Array

An instrumentation amplifier (the INA128P from Texas Instruments) was used to amplify the current signal and convert it to a voltage output in order to record the noise of the array after averaging. The average current of the array is copied using an NMOS mirror and connected externally to a 10 kΩ resistor (0.1% precision) and the amplifier's negative input, with the positive input biased. The amplifier reads the potential across the sense resistor V_S, and produces a voltage output with a gain of 250, meaning that an input current of 20 nA is equivalent to an output voltage of 50 mV. This test setup is shown in Fig. 7. The current measurement circuitry was powered by a pair of batteries and placed inside a Faraday cage along with the ASIC to reduce background noise. This signal was then connected via a shielded cable to the ADC to record the data and perform an FFT. The noise of the instrumentation amplifier according to the datasheet is less than 10 nV/$\sqrt{\text{Hz}}$ and 0.2 μV_{pp} at DC, but the amplifier noise has also been characterised and is shown with the results of the sensing array.

To characterise the full sensing array and processing module, a solution of distilled water was applied to the sensing surface and the reference electrode was biased such that the amplifier output read 50 mV, and therefore the current from the array and individual pixel was 20 nA. The results of this analysis are shown in Fig. 9 which plots the power spectral density for the individual pixel vs the averaged array. Coupling with the ring oscillator interferes with the higher frequency measurements, however we are most concerned with the low frequency variation that determines the ring oscillator frequency, so we shall only consider the output up to 1 kHz. The integrated noise up to 1 kHz is 75.6 μV and 160 μV for the array average and individual pixel respectively, showing that array averaging does reduce noise at the output. We can then refer the noise to the input by dividing by the array gain (made up of the amplifier gain, resistance R_S and the ISFET transconductance - in the case of the average, the divide by nine operation is cancelled by the summation of multiple noise samples). The
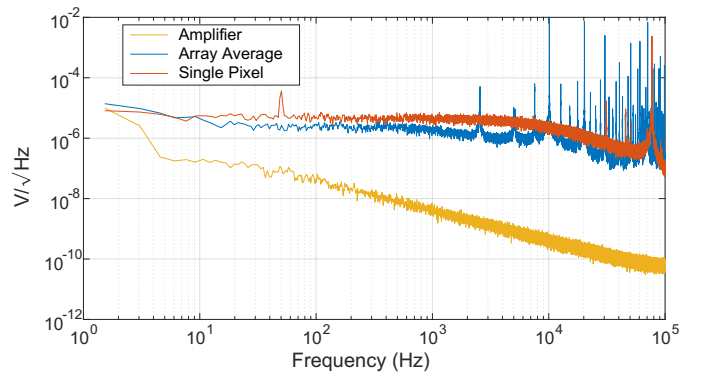

Fig. 9: Measured output noise of the sensor array compared to an individual pixel. The output instrumentation amplifier characterisation is shown for reference.

TABLE II: Array and Pixel Characteristics

Characteristic	Array	Pixel
Integrated Input Referred Noise up to 1 kHz (μV)	104	220
Minimum Detectable pH	0.008	0.017
Power Consumption at Biasing (Simulated) (nA)	189	21

input referred noise of the array is 104 μV, whereas for the individual pixel the figure is 220 μV.

D. pH Sensitivity

To test the pH sensitivity of the ASIC, pH buffers were used to apply a step change in pH. A flow cell was used to apply buffers continuously to the surface of the array [31]. This set-up can be seen in Fig. 10. Measurements were recorded using the Keithley 4200-SCS to read the output current sent to the ring oscillator through a current mirror. With a constant pH of 7 the reference electrode was biased such that the output current was 20 nA. A series of pH step changes were then injected into the flow cell and held over an extended period (> 120 seconds). The results of this can be seen in Fig. 11, which shows that the sensor produces a regular step with each pH change, corresponding to a very small section of the $I_d - V_{gs}$ curve, meaning that the steps in output current are almost linear (approximately 2.5 nA). This corresponds to a pH sensitivity of 13 mV/pH. This result is significantly lower from the theoretical result as discussed in Section II-D and this is likely due to an unwanted polyimide layer on the unmodified CMOS die. This layer increases the capacitive division of the charge that builds up on the floating gate and therefore reduces the sensitivity of the device. The polyimide layer can be removed in future processing runs to improve the sensitivity of the ISFET sensing array. From the sensitivity and the observed noise of the array (Section IV-C), the minimum detectable pH can be determined. The full array gives a detection limit of 0.008 pH, which is less than half that of an individual pixel, 0.017. These figures are summarised in the results Table II.

E. Thermoelectric Supply Investigation

The thermoelectric generators (TEGs) were characterised using an electrically heated surface (An SBH200D Block
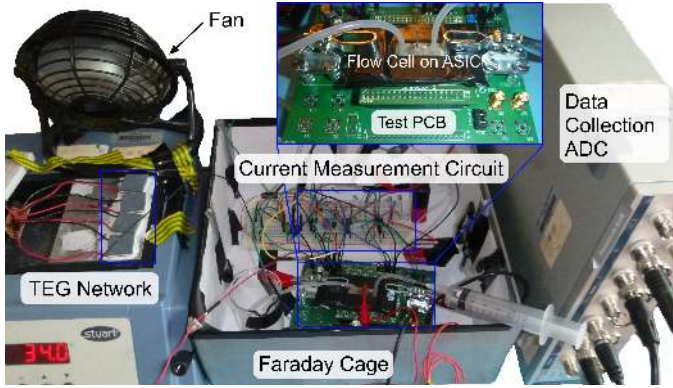
Fig. 10: The test set-up to measure noise of the ASIC and characterise the pH to frequency relationship of the system while it is thermally powered. An external circuit and ADC was used to perform and record the measurements.
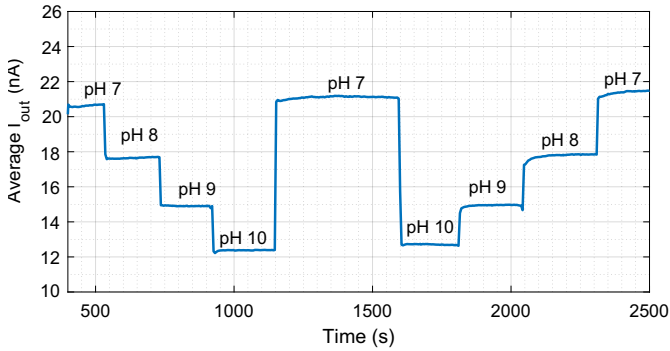

Fig. 11: A transient plot of step changes in pH buffers over time.

heater was used with an aluminium block), as shown in Fig. 10. The temperature was adjusted such that the metal surface was measured to be 29°C, approximate to skin temperature as discussed in Section II-C. The ambient temperature measured just above the TEG cold surface was initially 24°C. The TEGs were placed on to the surface with thermal grease to ensure a good connection, and small ceramic heat sinks were added, as discussed in Section II-A. Finally, a small DC fan was added to create a constant airflow over the device (measured to be approximately 1.5 m s^{-1} with a hand-held Tenma 72-6638 anemometer), causing the ambient temperature to drop to 23°C.

The open circuit voltage of the TEG network output ranged from approximately 200 to 220 mV which, once the chip was connected, dropped to an average of 55 mV. This is due to the input resistance of the LTC3108 which ideally would match to the source resistance of the power supply. However, as a series of TEGs was required to start the system reliably, the total source resistance of the TEG network is approximately 11 Ω, whereas at 55 mV the LTC3108 input resistance is approximately 3.5 Ω. As a result there is a voltage drop to 24% of the open circuit value. To improve the closed circuit input voltage, the resistance of the TEG network should be as close to the TEG input resistance as possible.

The supplied current was measured to be 6 mA, giving a total power output of 330 µW. With the efficiency of the

harvesting and regulation circuit being 15%, this suggests that the power available for the chip is 49.5 µW. This power is sufficient to supply the chip without the transmitter indefinitely. Under these conditions, the output voltage of the harvester reached 2.35 V in around 50 seconds, although the ASIC supply voltage reaches 1.2 V earlier as the regulator begins functioning above 1.6 V Turning the fan off reduced the power supplied to the chip to just 3.3 µW (after accounting for harvesting efficiency). At this level, the chip could not be run alone, but the stored energy could supply the chip for a further 4.5 minutes before the chip switches off.

The transmitter cannot be run continuously under the TEG power supply, however it is possible to duty cycle this module due to the separate supply in order to allow the TEG to recharge the 1500 µF storage capacitor while the transmitter is inactive. To calculate the achievable 'on' duration and duty cycle, the charge time and discharge current were used to find the charge and discharge times of the storage capacitor, for a given voltage drop (assuming this is going to provide the majority of the supply current when the transmitter is active). From observations we can see that the storage capacitor charges with a constant voltage (internally clamped to 5.25 V) by a Zenner diode) and discharges with a constant current of the transmitter. By solving these two equations for a permissible voltage drop on the storage capacitor, we can determine the maximum allowable transmit time and duty cycle. For a 1 mV drop in storage capacitor voltage from the maximum, the transmitter can be on for 5 ms every 10 seconds, a duty cycle of 0.05%.

F. Power Consumption Results

The power consumption of the ASIC is dependent on the pH voltage change, as such the figures for 0, 30 and 180 mV have been given in Table III to give a range of possible power consumptions. The results for sub-modules in the ASIC are given as simulated values and the top-level and transmitter are given as measured results. The measurements of the standalone ASIC were taken using the Keithley 4200-SCS.

These voltage steps represent the array bias point and using the sensitivity found in Section IV-D, we can say that a 30 mV step covers the expected operational range of our sensors. This means that the maximum power consumption of the sensing array and processing modules in normal body-worn operation is 6 µW, and can therefore be feasibly powered by a TEG. The transmitter as expected draws a significantly larger amount of power, however as suggested in Section IV-E this could be managed by using periodic transmission with a very low duty cycle in future designs.

G. Testing of Thermally Powered pH to Frequency Conversion

To test the full system, the ASIC and test PCB were connected to the TEG network as described in Section IV-E. The ambient room temperature was measured to be 24 °C with a fan creating an airflow, and the surface temperature of the aluminium block was approximately 29 °C. Under these conditions the TEG network produced a loaded voltage of 50 mV. The output of the instrumentation amplifier, V_o, and the

TABLE III: Power Consumption of ASIC Sub-modules

ASIC Sub-modules	Power Consumption		
$\Delta V_{chem} =$	Δ 0 mV	Δ 30 mV	Δ 180 mV
Single Pixel (Simulated)	50 nW	66 nW	313 nW
Pixel Array (Simulated)	509 nW	675 nW	2900 nW
Ring Oscillator (Simulated)	2.1 µW	2.5 µW	5.8 µW
Array Biasing (Simulated)	117 nW	117 nW	117 nW
Total of Sensing and Processing Modules (Measured)	4.96 µW	6.00 µW	17.21 µW
Transmitter Biasing (Simulated)	304.1 µW	304.1 µW	304.1 µW
Transmitter (On, Avg, Measured) (Off=0W)	1.91 mW	1.94 mW	2.3 mW

Fig. 13: The relationship between the output frequency and input pH of the ASIC.

TABLE IV: Specifications of the On-Body pH Sensing ASIC

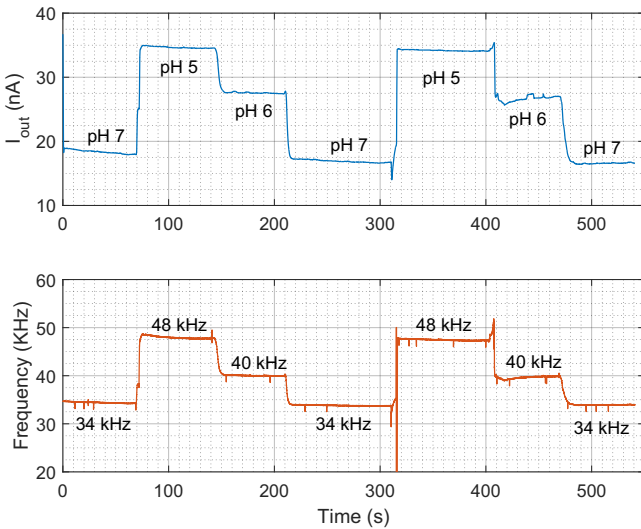| **Technology**	0.35 µm
Area	
Sensor and Processing	0.1089mm^2
Transmitter	0.0128mm^2
Supply Voltage (VDD)	1.2 V
Power Consumption	(At biasing of 20 nA)
Single Pixel (Simulated)	50 nW
Pixel Array (Simulated)	509 nW
Ring Oscillator (Simulated)	2.1 µW
Array Biasing (Simulated)	117 nW
Total ASIC (Exc. Transmitter, Measured)	4.96 µW
Transmitter (On, Avg., Measured)	1.91 mW
Region of Operation	Weak inversion
Number of Sensors	9
Sensor Area	55 x 65 µm^2
pH Sensitivity	13 mV/pH
Input Referred Noise	104.1 µV
Minimum Detectable pH	0.008 pH

Fig. 12: A transient plot of changes in output frequency of ring oscillator with changes in pH, with frequencies (to the nearest kHz) annotated. The system was powered by a series of TEGs during the test.

output of the ring oscillator buffer were captured by an ADC. The sensing array was biased as described in Section IV-A. Successive step changes in pH were injected through the flow cell while the frequency of the output buffer was measured. Fig. 12 shows the plots corresponding to the measured current and frequency of the ring-oscillator against time for a pH range of 7 to 5. The frequency over this spread ranges from 34 to 52 kHz, with a sensitivity of 6 to 8 kHz/pH, which shows suitability for detection of expected physiological on-body pH ranges as discussed in Section II-D. The relationship between frequency and pH is plotted in Fig. 13. This calibration allows us to predict the frequency output of the processing module for a given pH and consequently calculate the pH from the received modulated signal.

V. CONCLUSIONS

This paper has presented the first thermally powered, low-power, low-noise, integrated pH measurement ASIC for on-body applications using an array of ISFETs, supported by
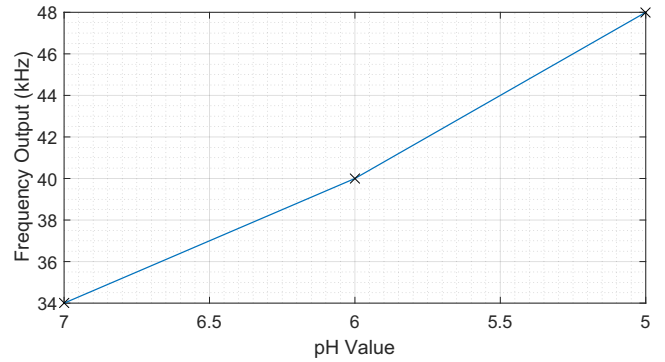
design considerations for an on-body thermally powered device and evaluation of thermoelectric generators (TEGs) for this application. The ASIC has been manufactured in a 0.35µm CMOS process and tested *in-vitro*, with a summary of achieved specifications shown in Table IV. The sensing and processing modules are shown to consume no more than 6 µW, and consequently the feasibility of obtaining pH measurements through harvesting body heat has been proved. Furthermore, the implementation of array averaging has been shown to enable an input referred noise of 104 µV (up to 1 kHz) and a minimum detectable pH of 0.008 pH, which are lower than those obtained when using a single sensor only. These improvements in sensitivity facilitate the weak inversion operation of the sensors which facilitates the low power budget required when harvesting thermal energy from the body. The system has been tested on pH 7 to 5, a range equivalent to that found in perspiration on the epidermis. The sensitivity of the ASIC during these tests was found to be 6 to 8 kHz.

This work is the first to present and analyse the requirements for a thermally powered body-worn electrochemical sensor and provides a functional proof-of-concept towards the development of wearable ISFET arrays powered by body heat for on-body pH measurements. The system pushes towards the goal of continuous, low-cost and non-invasive chemical

measurements in sports science and healthcare. The ASIC has been shown to reliably provide pH measurements for on-body analysis of chemicals such as perspiration and is now ready for testing *in-vivo*. This will be achieved by integrating the ASIC into wearable bandage which will allow the TEG network and sensors to wrap around the arm. In the short term, this can be used to obtain pH measurements during exercise, indicating hydration levels and other biochemical imbalances in real time.

APPENDIX
MODELS USED TO ANALYSE A BODY WORN TEG

To choose an appropriate TEG for a body worn application, an equivalent thermal model of the environment can be used. The simple model used here is presented by Lossec *et.al.* [18], which is appropriate as we are using this as a guide to select a TEG. Suarez *et.al.* provide a more comprehensive analysis of wearable thermoelectric energy harvesters [19]. The simplified thermal model is shown in Fig. 14a and contains the body, TEG and ambient thermal impedance in series (R_{th_B}, R_{th_G} and R_{th_A} respectively), allowing us to calculate the temperature differential across the generator, ΔT_G [18]. We wish to maximise this temperature difference as it is directly proportional to the output voltage of the TEG.
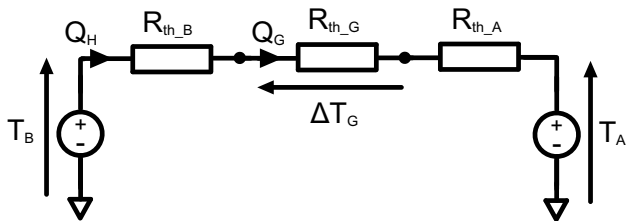
(a) Equivalent model of a thermal system, showing the relationship between the body, TEG and ambient temperatures.
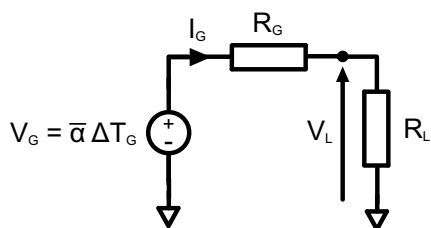
(b) The equivalent model of the electrical properties of a TEG. The dependence of output voltage V_L is determined by the output

Fig. 14: Equivalent models for designing a thermoelectric system.

The heat transfer coefficient, in $\mathrm{W\,m^{-2}\,K^{-1}}$, allows us to calculate the thermal impedance of a surface for a given area through Eq.3, where R_{th} is thermal impedance, h is the heat transfer coefficient and S_{th} is the surface area through which heat is transferred. The worst case coefficients for the human body and air are reportedly 20 and 9.7 $\mathrm{W\,m^{-2}\,K^{-1}}$ respectively [18], which allows us to calculate the thermal impedances R_{th_B} and R_{th_A} for a given TEG surface area in our model.

$$R_{th} = \frac{1}{hS_{th}} \tag{3}$$

As R_{th_A} is usually quite high, so it is generally accepted that a miniature heat sink will be required to reduce this impedance and therefore increase the ΔT_G such that it is able to power the load component, which can be calculated using Eq.4.

$$\Delta T_G = \frac{R_{th_G}}{R_{th_B} + R_{th_A} + R_{th_G}} \times (T_B - T_A) \tag{4}$$

To determine the maximum power that a TEG can produce, the electrical properties of the generator and load must also be considered. This model is shown in Fig. 14b, which illustrates that the open circuit voltage, V_G is proportional to the temperature gradient across the TEG through the seebeck coefficient, $\bar{\alpha}$. As stated previously, in on-body applications ΔT_G is low and so the voltage produced by a TEG is usually in the order of millivolts, already far lower than the supply requirements of a typical electrical circuit. Furthermore, reaching the maximum power output of a TEG depends on matching the load to the source resistance, and consequently voltage supplied is half the open circuit voltage. This further exacerbates the problem of operating with very low supply voltages, therefore a step-up converter is required.

REFERENCES

[1] S. Imani, P. P. Mercier, A. J. Bandodkar, J. Kim, and J. Wang, "Wearable Chemical Sensors: Opportunities and Challenges," in *Proc. IEEE Int. Symp. on Circuits and Syst. (ISCAS)*, May 2016 , pp. 1122–1125.

[2] S. Imani, A. J. Bandodkar, A. M. V. Mohan, R. Kumar, S. Yu, J. Wang, and P. P. Mercier, "A wearable chemicalelectrophysiological hybrid biosensing system for real-time health and fitness monitoring," *Nature Communications*, vol. 7, no. May, p. 11650, 2016.

[3] Z. Sonner, E. Wilder, J. Heikenfeld, G. Kasting, F. Beyette, D. Swaile, F. Sherman, J. Joyce, J. Hagen, N. Kelley-Loughnane, and R. Naik, "The microfluidics of the eccrine sweat gland, including biomarker partitioning, transport, and biosensing implications." *Biomicrofluidics*, vol. 9, no. 3, p. 031301, 2015.

[4] A. J. Bandodkar and J. Wang, "Non-invasive wearable electrochemical sensors: A review," *Trends in Biotechnology*, vol. 32, no. 7, pp. 363–371, 2014.

[5] A. Cazale, W. Sant, J. Launay, F. Ginot, and P. Temple-Boyer, "Study of field effect transistors for the sodium ion detection using fluoropolysiloxane-based sensitive layers," *Sensors and Actuators, B: Chemical*, vol. 177, pp. 515–521, 2013.

[6] H. Y. Y. Nyein, W. Gao, Z. Shahpar, S. Emaminejad, S. Challa, K. Chen, H. M. Fahad, L. C. Tai, H. Ota, R. W. Davis, and A. Javey, "A Wearable Electrochemical Platform for Noninvasive Simultaneous Monitoring of Ca2+ and pH," *ACS Nano.*, vol. 10, no. 7, pp. 7216–7224, 2016.

[7] G. Matzeu, C. O'Quigley, E. McNamara, C. Zuliani, C. Fay, T. Glennona, and D. Diamond, "An integrated sensing and wireless communications platform for sensing sodium in sweat," *Analytical Methods*, vol. Advance Ar, pp. 64–71, 2016.

[8] D. Rose, J. Prendergast, M. Ratterman, D. Griffin, L. Hou, N. Kelley-Loughnane, R. Naik, J. Hagen, I. Papautsky, and J. Heikenfeld, "Adhesive RFID Sensor Patch for Monitoring of Sweat Electrolytes." *IEEE Trans. Biomed. Eng.*, vol. 62, no. 11, pp. 46–63, 2014.

[9] W. Gao, S. Emaminejad, H. Y. Y. Nyein, S. Challa, K. Chen, A. Peck, H. M. Fahad, H. Ota, H. Shiraki, D. Kiriya, D.-H. Lien, G. A. Brooks, R. W. Davis, and A. Javey, "Fully integrated wearable sensor arrays for multiplexed in situ perspiration analysis," *Nature*, vol. 529, no. 7587, pp. 509–514, 2016.

[10] H. Lee, T. K. Choi, Y. B. Lee, H. R. Cho, R. Ghaffari, L. Wang, H. J. Choi, T. D. Chung, N. Lu, T. Hyeon, S. H. Choi, and D.-H. Kim, "A graphene-based electrochemical device with thermoresponsive microneedles for diabetes monitoring and therapy," *Nature Nanotechnology*, vol. 11 no. 6, pp.566–572, Jun. 2016.

[11] W. Jia, A. J. Bandodkar, G. Valdés-Ramírez, J. R. Windmiller, Z. Yang, J. Ramírez, G. Chan, and J. Wang, "Electrochemical tattoo biosensors for real-time noninvasive lactate monitoring in human perspiration," *Analytical Chemistry*, vol. 85, no. 14, pp. 6553–6560, 2013.

[12] P. Georgiou and C. Toumazou, "ISFET characteristics in CMOS and their application to weak inversion operation," *Sensors and Actuators, B: Chemical*, vol. 143, no. 1, pp. 211–217, 2009.

[13] N. Moser, T. S. Lande, C. Toumazou, and P. Georgiou, "ISFETs in CMOS and Emergent Trends in Instrumentation: A Review," *IEEE Sensors J.*, vol. 16, no. 17, pp. 6496–6514, 2016.

[14] S. Nakata, T. Arie, S. Akita, and K. Takei, "Wearable, flexible, and multifunctional healthcare device with an ISFET chemical sensor for simultaneous sweat pH and skin temperature monitoring," *ACS Sens.*, vol. 2, no. 3, pp. 443-448, 2017.

[15] V. Leonov, T. Torfs, P. Fiorini, and C. Van Hoof, "Thermoelectric converters of human warmth for self-powered wireless sensor nodes," *IEEE Sensors J.*, vol. 7, no. 5, pp. 650–656, 2007.

[16] P. D. Mitcheson, "Energy harvesting for human wearable and implantable bio-sensors," *2010 Annu. Int. Conf. of the IEEE Engineering in Medicine and Biology Society, EMBC'10*, pp. 3432–3436.

[17] P. Webb, "Temperatures of skin, subcutaneous tissue, muscle and core in resting men in cold, comfortable and hot conditions," *European Journal of Applied Physiology and Occupational Physiology*, vol. 64, no. 5, pp. 471–476, 1992.

[18] M. Lossec, B. Multon, H. Ben Ahmed, and C. Goupil, "Thermoelectric generator placed on the human body: system modeling and energy conversion improvements," *Eur. Phys. J. Appl. Phys*, vol. 52, no. 1, pp. 11103, 2010.

[19] F. Suarez, A. Nozariasbmarz, D. Vashaee, and M. C. Öztürk, "Designing thermoelectric generators for self-powered wearable electronics," *Energy Environ. Sci.*, vol. 9, no. 6, pp. 2099–2113, 2016.

[20] K. Sato, W. H. Kang, K. Saga, and K. T. Sato, "Biology of sweat glands and their disorders. I. Normal sweat gland function." *Journal of the American Academy of Dermatology*, vol. 20, no. 4, pp. 537–563, 1989.

[21] M. J. Patterson, S. D. Galloway, and M. a. Nimmo, "Variations in regional sweat composition in normal human males." *Experimental physiology*, vol. 85, no. 6, pp. 869–875, 2000.

[22] J. Bausells, J. Carrabina, A. Errachid, and A. Merlos, "Ion-sensitive field-effect transistors fabricated in a commercial CMOS technology," *Sensors and Actuators, B: Chemical*, vol. 57, no. 1-3, pp. 56–62, 1999.

[23] P. A. Hammond and D. R. S. Cumming, "Performance and system-on-chip integration of an unmodified CMOS ISFET," *Sensors and Actuators, B: Chemical*, vol. 111-112, pp. 254–258, 2005.

[24] L. Shepherd, P. Georgiou, and C. Toumazou, "A novel voltage-clamped CMOS ISFET sensor interface," in *Proc. IEEE Int. Symp. Circuits Syst. (ISCAS)*, May 2007, pp. 3331-3334.

[25] S. Martinoia and G. Massobrio, "Behavioral macromodel of the ISFET in SPICE," *Sensors and Actuators, B: Chemical*, vol. 62, no. 3, pp. 182–189, 2000.

[26] L. Shepherd and C. Toumazou, "Weak Inversion ISFETs for ultra-low power biochemical sensing and real-time analysis," in *Sensors and Actuators, B: Chemical*, vol. 107, no. 1 SPEC. ISS., pp. 468–473, 2005.

[27] P. Georgiou and C. Toumazou, "CMOS-based programmable gate IS-FET," *Electronics Letters*, vol. 44, no. 22, pp. 1289 - 1290, 2008.

[28] Y. Liu, P. Georgiou, T. Prodromakis, T. G. Constandinou, and C. Toumazou, "An Extended CMOS ISFET Model Incorporating the Physical Design Geometry and the Effects on Performance and Offset Variation," *IEEE Tran. Electron Devices*, vol. 58, no. 12, pp. 4414–4422, 2011.

[29] S. Suman, K. G. Sharma, and P. K. Ghosh, "Analysis and Design of Current Starved Ring VCO," in *Int. Conf. Elect., Electron. and Optimization Techniques (ICEEOT)*, Mar. 2016, pp. 3222–3227.

[30] Y. T. Liao, H. Yao, A. Lingley, B. Parviz, and B. P. Otis, "A 3-uW CMOS glucose sensor for wireless contact-lens tear glucose monitoring," *IEEE J. Solid-State Circuits*, vol. 47, no. 1, pp. 335–344, 2012.

[31] Y. Hu and P. Georgiou, "A robust ISFET pH-measuring front-end for chemical reaction monitoring," *IEEE Trans. Biomed Circuits Syst*, vol. 8, no. 2, pp. 177–185, 2014.

Matthew Douthwaite (S'14) received the M.Eng. degree in electrical and electronic engineering and the M.Res. degree in advanced computing from Imperial College London (ICL), London, U.K., in 2015 and 2016, respectively.

He is currently pursuing the Ph.D. degree with the EPSRC Centre for Doctoral Training in High Performance Embedded and Distributed Systems, within the Centre for Bio-Inspired Technology, Department of Electrical and Electronic Engineering, Imperial College London. He received the Usmani Prize for Micro-electronics in 2014 for outstanding performance in examinations in the area of micro-electronics and the Kenneth Camm Prize in 2013 for outstanding achievement alongside an overseas engineering voluntary project. His research interests include the design of ultra low power bio-inspired analogue integrated circuits, particularly for wearable applications and energy harvesting.

Ermis Koutsos (S'12) received the BSc degree in Electrical and Electronic Engineering from University of Surrey, U.K. in 2011 and the MSc in analogue and digital integrated circuit design and the Ph.D. degree from the Dept. of Electrical and Electronic Engineering of Imperial College London, U.K., in 2012 and 2016, respectively. His research interest focuses on the design of low power mixed signal electronics for biomedical applications. Mr. Koutsos is a scholar of EPSRC.

David C. Yates (M'03) received the M.Eng. degree in electrical engineering and the Ph.D. degree in ultra low power RF circuit and antenna design for wireless sensor networks from the Imperial College London, London, U.K., in 2001 and 2007, respectively.

His doctoral research was focused on ultralow-power wireless links. He is currently a Research Fellow with the Control and Power Group, Department of Electrical and Electronic Engineering, Imperial College London. His research interests include converters and magnetics for wireless power transfer and ultralow-power RF circuits for sensor networks.

Paul D. Mitcheson (SM'12) received the M.Eng. degree in electrical and electronic engineering and the Ph.D. degree in micro-power motion based energy harvesting for wireless sensor networks from the Imperial College London, London, U.K., in 2001 and 2005, respectively.

He is currently a Professor in Electrical Energy Conversion with the Control and Power Research Group, Electrical and Electronic Engineering Department, Imperial College London. His research interests include energy harvesting, power electronics, and wireless power transfer to provide power to applications in circumstances where batteries and cables are not suitable. His research has been supported by the European Commission, Engineering and Physical Sciences Research Council, and several companies.

Prof. Mitcheson is a Fellow of the Higher Education Academy and is on the executive committee of the UK Power Electronics Centre.

Pantelis Georgiou (AM'05-M'08-SM'13) received the M.Eng. degree in electrical and electronic engineering and the Ph.D. degree from Imperial College London (ICL), London, U.K., in 2004 and 2008, respectively.

He is currently a Reader with the Department of Electrical and Electronic Engineering, ICL, where he is also the Head of the Bio-Inspired Metabolic Technology Laboratory, Centre for Bio-Inspired Technology. His research includes bio-inspired circuits and systems, CMOS based Lab-on-Chip technologies, and application of microelectronic technology to create novel medical devices. He has made significant contributions to integrated chemical-sensing systems in CMOS, conducting pioneering work on the development of ISFET sensors, which has enabled applications, such as point-of-care diagnostics and semiconductor genetic sequencing and has also developed the first bio-inspired artificial pancreas for treatment of Type I diabetes using the silicon-beta cell. He received the IET Mike Sergeant Medal of Outstanding Contribution to Engineering in 2013. He is a member of the IET and serves on the BioCAS and Sensory Systems technical committees of the IEEE CAS Society. He is also the CAS representative on the IEEE Sensors council and the IEEE Distinguished Lecturer in Circuits and Systems.